Design of a Reconfigurable Optical Computing Architecture Using Phase Change Material

Parya Zolfaghari, Sébastien Le Beux

Design of A Reconfigurable Optical Computing Architecture Using Phase Change Material

Parya Zolfaghari and Sébastien Le Beux

Department of Electrical & Computer Engineering
Concordia University
Montreal, Canada

p_zolfag@encs.concordia.ca, slebeux@encs.concordia.ca

Abstract. Silicon photonics is an emerging technology allowing to take the advantage of high-speed light propagation to accelerate computing kernels in integrated systems. Micrometer-scale optical devices call for reconfigurable architectures to maximize resources utilization. Typical reconfigurable optical computing architectures involve micro-ring resonators for electro-optic modulation. However, such devices require voltage and thermal tuning to compensate for fabrication process variability and thermal sensitivity. This power-hungry calibration leads to significant static power overhead, thus limiting the scalability of optical architectures. In this chapter, we propose to use non-volatile Phase Change Materials (PCM) elements to route optical signals only through the required resonators, hence saving calibration energy of bypassed resonators. The non-volatility of PCM elements allows maintaining the optical path. We investigate the efficiency of the PCM elements on the Reconfigurable Directed Logic (RDL) architecture. We also evaluate the static power saving induced by the use of couplers instead of microring to redirect WDM signals into a single waveguide. Finally, we show that the couplers can be efficiently used to cascade the architectures, allowing to increase the number of inputs to be processed without opto-electronic conversions. Compared to a ring-based implementation of RDL architecture, results show that the proposed implementation allows reducing the static power by 53% on average.

Keywords: Nanophotonics, Phase Change Material (PCM), Reconfigurable computing architectures.

1 Introduction

Silicon photonics have attracted attention due to the compatibility with CMOS manufacturing process. The technology allows integrating high speed photonic devices to provide high bandwidth low latency chip scale interconnects [1][2]. As the technology continues to mature, emerging optical computing architectures are developed to accelerate neural networks applications [3] and microwave processing [4]. The design of optical circuits dedicated to matrix multiplications, logic functions [5] and ad-

ders [6] are also investigated. Logic circuits relying on integrated optics involve electro-optic devices such as micro-ring resonators. In [7][8] the rings are organized as an array of optical switches to control light propagation. Such architecture allows to simultaneously controlling switching operation of the rings, which lead to low latency processing. Reconfigurable optical architectures [9][10] allow to efficiently use, bulky, optical devices for multiple operation, thus allowing to reduce the cost overhead induced by the technology. A feature shared by such architecture is the need to calibrate ring resonators in order to control optical signal transmissions. While high contrast can be achieved, the method requires voltage and thermal tuning to calibrate the rings, which accounts for up to 40% [10] of the static power consumption. Disruptive materials and architectures are thus needed to overcome the low energy efficiency of optical devices calibration. Phase Change Material (PCM) has been widely studied to design non-volatile photonic circuits such as neural networks [11]. Indeed, the non-volatility of PCM based devices allows to maintain the configuration of optical device without consuming energy. Typical configurations involve amorphous (am) and crystalline (cr) states, which can be obtained by heating the device [12]. Among recently demonstrated PCM based devices, a Directional Coupler (DC) reported in [13] leads to 0.16dB and 0.72dB attenuation under cr and am states respectively at wavelength 1521.5nm. Such low attenuation and the associated high optical contrasts allow to envision new optical architectures involving reconfigurable optical paths. In this chapter we propose an optical architecture allowing to bypass unused optical devices. To achieve this, PCM-based directional couplers are placed before and after resonating devices, thus allowing either to transmit optical signals to devices for modulation purpose or to bypass them. The use of the bypass path allows to avoid calibration of the optical devices, thus leading to significant reduction in the static power consumption. We investigate the efficiency of the proposed design on the RDL architecture. We also investigate the cascading of the proposed cell using directional couplers combined with lasers source placed between the cells. The architecture involves the use of coupler which induces loss resulting in laser power overhead.

To evaluate the proposed architectures, we define a loss model allowing to estimate the laser power overhead and the reduced ring calibration power consumption. We also investigate the impact of the architecture reconfiguration frequency on the power saving. Results show coupler based implementation of PCM based RDL leads to 53% of static power reduction compared with baseline while ring based implementation of RDL shows 19% of saving.

The chapter is organized as follows. Section 2 presents an overview of micro ring resonator-based computing architectures and introduces PCM based photonic devices. In Section 3, we present the proposed reconfigurable PCM-based architecture. Section 4 describes the power model and Section 5 presents results and discusses the cascading of the proposed architecture for multi-input logic. Section 6 concludes the work.

2 Related Work

In this section we present works related to optical computing architectures and the application of PCM in nanophotonic circuits.

2.1 Optical Computing Architectures

Numerous optical accelerators have been designed to execute both arithmetic and logic operation. They involve key optical devices such as micro rings, micro-disks, photonic crystal cavities and waveguides. A common objective is to reduce the critical path delay, which can be obtained by simultaneously applying multiple electro-optic modulation on optical signals propagating along a waveguide. By doing so, an 8-bit ripple carry adder with a 20ps critical path delay has been demonstrated in [14]. The same approach has been used in [15] for the design of an n-bit multiplier. Directed logic (DL) architectures have been proposed to efficiently utilize optical devices by simultaneously executing AND and NAND [16], the outputs being available on through port and drop port of a ring resonator. The approach has then been extended to XOR and XNOR operations [17]. A key issue with the above-mentioned architectures is the limited number of operations that can be executed, which is solved by the Reconfigurable Directed Logic (RDL) [10]. The RDL involves parallel waveguides on which modulators are serially placed, thus allowing to map sum-of-product functions. To do so, the architecture relies on modes (named pass/pass, pass/block, block/pass and block/block) which are configured by calibrating the modulator using thermal tuning. Hence, the main drawback of the architecture is the need to constantly thermally tuning ring resonators, even if no modulation is carried out, which is power consuming. In [22], we solved the problem by using PCM based directional couplers [13]. The directional couplers allow to bypass rings when no modulation is needed, thus avoiding to thermally tuning unused modulators. We investigated the efficiency of PCM based DC on RDL architecture. Results showed an average power saving of 32.8% and architecture is more power efficient for frequencies lower than 158 KHz. In this chapter we investigate the power consumptions of RDL in [10] and our proposed RDL [22] taking into account the power consumed by filter rings. We also extend the architecture to support multi-inputs logic through a cascading of the reconfigurable cells.

2.2 Phase Change Material (PCM)

The use of Phase-Change Material (PCM) in photonic platforms has been widely studied in recent years. Indeed, sub-nanosecond phase transition, femtojoule-scale phase transition energy consumption, 10^{15} switching cycle endurance and years long state retention have provided the ground for the massive deployment of PCM in numerous applications. Crystalline and amorphous states show significant differences in optical properties [12][18]. Hence, binary applications such as memory set and reset can be achieved using phase transition of PCM, which is obtained by thermal annealing using external heaters, optical pulses or electrical pulses [12]. The use of interme-

diate phase levels, i.e. not fully crystalline or amorphous, leads to multi-level memories [19] and weighting functions in spiking neural networks [11]. PCM is also commonly used for on-chip optical routing applications due to the high optical contrast they provide. For instance, an optical switch based on GST (germanium-antimony-tellurium) sandwiched between the branches of a directional coupler is reported in [20]. In the design, amorphous and crystalline states of the GST lead to cross and bar transmission of optical signals respectively. The design has been further improved in [13] in order to reach 0.16dB and 0.72dB Insertion Loss (IL) for cross and bar transmissions respectively. Low transmission loss and non-volatility are the key characteristics of the directional coupler we are using to bypass unused modulators in the proposed architectures.

3 Proposed Cell

In this section, we first present an overview of the proposed reconfigurable logic cell. We then detail the cell configurations according to the state of the PCM elements and the detuning of the ring resonator. The implementation of the AND is presented using the proposed cell and finally, we present two implementations of the RDL involving the proposed cell.

3.1 Cell Overview

The proposed cell is composed of two phase change Directional Coupler (DC_1 and DC_2) and one micro ring resonator, as shown in Figure 1. The state of the PCM in DC is electrically configured using a dedicated control signal. As defined in Section 3, cross and bar are obtained for Amorphous (Am) and Crystalline (Cr) states respectively. Depending on the state of DC_1, two signal paths can be configured: i) modulation is obtained for Cr state and ii) bypass is obtained for Am state. In the modulation path, the optical signal propagates through a micro ring resonator, where modulation of the input data is carried out, before reaching DC_2. In the bypass path, the optical signal directly propagates towards DC_2. Depending on the state of DC_2, signals are transmitted either to the output of the cell or to a terminator.

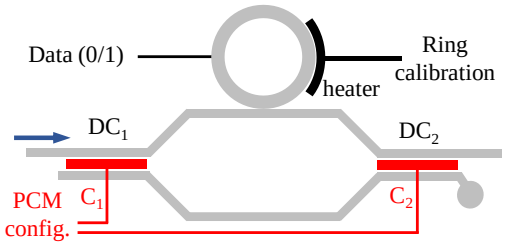

Figure 1: Proposed cell based on micro ring resonator and phase change directional coupler

The cell is configured according to i) the state of the PCM elements in the DCs and ii) the tuning of the ring. By combining the states of the PCM and ring tuning, the following cell configurations are defined:

- Pass/Pass: Both DC_1 and DC_2 are in the Amorphous state as shown in Figure 2.a. The input signal propagates through the bypass path and is transmitted to the output. Since the signal does not propagate through modulation path, no thermal calibration of the ring is needed.
- Block/Block: Figure 2.b represents the block/block mode. Similarly to pass/pass mode, the signal propagates through the bypass path since DC_1 is set to the amorphous state. However, instead of transmitting the signal to the output, DC_2 is configured to the crystalline state, which leads to a transmission of the signal to the terminator. Hence, the optical signal is strongly attenuated on the output.
- Pass/block: The input signal is transmitted to the modulation path, which is achieved with DC_1 is configured in the crystalline state as shown in Figure 2. c. The signal is first modulated by the input data and is then transmitted to the output (DC in crystalline state). Since a modulation occurs, the ring is thermally calibrated to the signal wavelength (λ_s). Therefore, data input '0' leads to the coupling of the signal, which results in a strong attenuation, while data input '1' detunes the resonance of the ring, which leads to a high transmission of the signal.
- Block/Pass: Similarly, to Pass/block, the signal propagates through the modulation path, as illustrated in Figure 2.d. However, the ring is tuned to $\lambda_s - \Delta_\lambda$, i.e. the ring is off signal resonance for data input '0'. Data input '1' leads to a red shift of the ring and hence a strong attenuation of the optical signal.

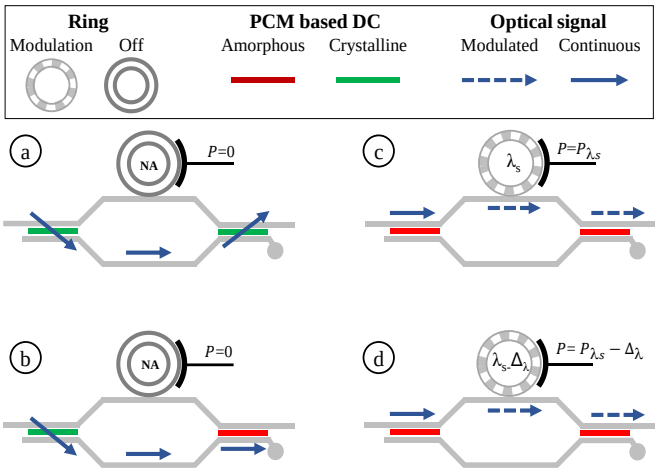

Figure 2: Non-volatile implementation of a) pass/pass. b) block/block. c) pass/block d) block/pass modes from RDL[10] using PCM-based directional couplers

3.2 Implementation of AND Function

In order to implement the multiplication of two operands, the cell is cascaded as shown in Figure 3. To reduce the design complexity, DC_2 from the first cell is merged with DC_1 from the second cell. Hence, the configuration of block/block mode is only available in the second cell, which implies to configure the first cell in the pass/pass mode. The design allows to implement functions such as A, B, AB, AB'. Figure 3 illustrates the implementation of AB'. For this purpose first and second cells are configured in pass/block and block/pass modes respectively. This is obtained by configuring DC_1, DC_2 and DC_3 in crystalline state and tuning the first and second cell to λ_0 and $\lambda_0-\Delta_\lambda$ respectively .

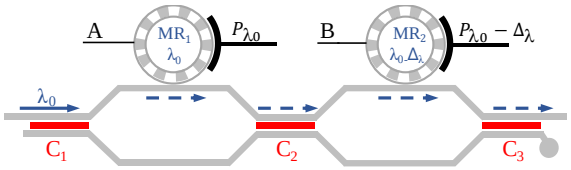

Figure 3: Implementation of AB'

3.3 Non-Volatile RDL Architecture

In order to implement the function OR, the architecture in Figure 3 is duplicated on two parallel waveguides. Signals propagating from waveguides are transmitted to multiband photo detector which results in the sum of products.

Proposed PCM based RDL architecture feature the implementation of XOR function, i.e. AB'+BA', with AB' being implemented in the upper waveguide. It is obtained by configuring first and second cell in pass/block and block/pass modes respectively. This is achieved by configuring DC_1, DC_2 and DC_3 in crystalline states and tuning the first and second rings to λ_0 and $\lambda_0-\Delta_\lambda$ respectively. Therefore, signal at λ_0 is transmitted to the output when rings are off resonance, which requires A=1 and B=0. BA' is implemented on the lower waveguide by configuring first and second cells in block/pass and pass/block modes respectively.

In the following, we present two non-volatile implementations of the RDL architecture as illustrated in Figure 4.a and Figure 4.b.

- Ring filter based RDL (Figure 4.a): The MRR filters on the left-hand side are used to couple signal from lasers to the horizontal waveguides. The modulated signals are transmitted to a photo detector through MRRs located on the right-hand side. The filter MRRs require constant calibration.
- Coupler based RDL (Figure 4.b): Lasers are placed on each waveguide allowing to turn them off when signal is not used. Therefore block/block mode is not needed which allows to remove the terminator. Signals propagating from two waveguides are merged through coupler.

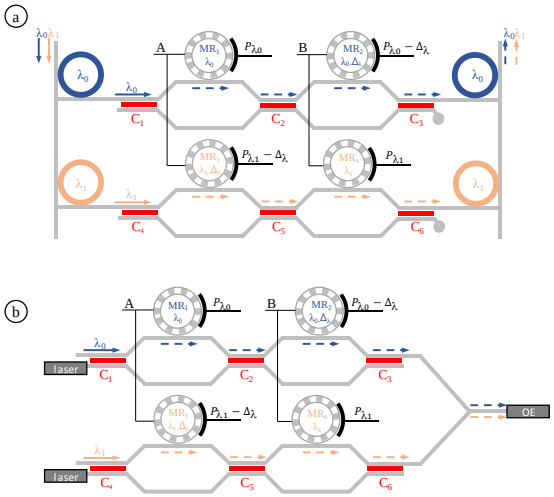

Figure 4: Configuration of RDLs for XOR, a) Ring filter based RDL, b) coupler based RDL

Table 1 summarizes the configurations of PCMs and the rings according to the logic function for filter ring based RDL architecture. Functions involving a single product induce block/block mode for the lower waveguide which leads to bypassing of signal. XOR and XNOR functions involve modulation on all the rings, which requires to configure all the DCs in the cr state. MR_3 modulates data when functions involving a second product include operand 'A' (e.g. XOR and XNOR). Since all functions can be executed without reconfiguring DC_6, the device could be removed for reduced hardware complexity purpose. However, since keeping DC_6 offers the opportunity to map single produce function on the lower waveguide, we didn't consider this optimization.

Table 1: Device state according to the configured function for RDL with PCM and filter rings

Device	Functions						
	A	B	AB	AB'	$A+B$	$A+B'$	$AB+A'B'$
DC_1	cr	am	cr	cr	cr	cr	cr
DC_2	am	am	cr	cr	am	am	cr
DC_3	am	cr	cr	cr	am	am	cr
MR_1	λ_0	off	λ_0	λ_0	λ_0	λ_0	λ_0
MR_2	off	λ_0	λ_0	$\lambda_0-\Delta_\lambda$	off	off	λ_0
DC_4	am	am	am	am	am	am	cr
DC_5	cr	cr	cr	cr	am	am	cr
DC_6	cr	cr	cr	cr	cr	cr	cr
MR_3	off	off	off	off	off	off	$\lambda_1-\Delta_\lambda$
MR_4	off	off	off	off	λ_1	$\lambda_1-\Delta_\lambda$	$\lambda_1-\Delta_\lambda$

Table 2 summarizes the PCM configuration and ring tuning for coupler based RDL. Laser is turned off on lower waveguide for functions involving the use of one waveguide such as A, AB. This allows to avoid the configuration of PCMs which are shown with don't care (i.e. x) in the table.

Table 2: Device state according to the configured function for RDL with PCM and coupler

Device	Functions						
	A	B	AB	AB'	$A+B$	$A+B'$	$AB+A'B'$
DC_1	cr	am	cr	cr	cr	cr	cr
DC_2	am	am	cr	cr	am	am	cr
DC_3	am	cr	cr	cr	am	am	cr
MR_1	λ_0	off	λ_0	λ_0	λ_0	λ_0	λ_0
MR_2	off	λ_0	λ_0	$\lambda_0-\Delta_\lambda$	off	off	λ_0
DC_4	x	x	x	x	am	am	cr
DC_5	x	x	x	x	am	am	cr
DC_6	x	x	x	x	cr	cr	cr
MR_3	off	off	off	off	off	off	$\lambda_1-\Delta_\lambda$
MR_4	off	off	off	off	λ_1	$\lambda_1-\Delta_\lambda$	$\lambda_1-\Delta_\lambda$

4 Power Model

In this section, we present the proposed power model. It takes into account the power consumption of i) lasers, ii) rings resonators and iii) PCM, as defined by:

$$P\_total = P\_laser + P\_ring + P\_reconfig \quad (1)$$

Where *P_laser* is the laser power needed to reach the targeted optical power. *P_ring* is power consumption induced by both ring tuning and data modulation. *P_reconfig* corresponds to the power consumption required to change the state of the PCMs when the architecture is reconfigured.

4.1 Laser Power

The optical signals propagating through the architecture experience losses induced by micro ring resonator and directional coupler. The worst-case Insertion Loss (IL_{wc}) allows estimating the laser power consumption according to the received power ($P_{received}$) and the laser efficiency (*eff*), as defined by:

$$P_{laser}=(P_{received}+IL_{wc})/eff \quad (2)$$

We estimate the losses for each device of the architecture as follows:

$$IL_{wc}=IL_{ring}+IL_{DC}+IL_{coupler} \quad (3)$$

$$IL_{ring}=\sum_{m=1}^{M} IL_{\lambda s}+\sum_{n=1}^{N} IL_{\lambda s-\Delta\lambda} \quad (4)$$

$$IL_{DC}=\sum_{k=1}^{K} IL_{cr}^{bar}+\sum_{f=1}^{F} IL_{am}^{cross} \quad (5)$$

where IL_{ring} ,IL_{DC} and $IL_{coupler}$ are the ring, DC and coupler losses respectively. M and N are the number of rings tuned to λ_s and $\lambda_s-\Delta_\lambda$ respectively. K is the number of bar transmission for PCM configured in *cr* state and F is the number of cross transmissions for PCM in *am* state. As previously explained, *am* state leads to the cross transmission of most signal power (IL_{am}^{cross}) while only small fraction of the power is transmitted to bar (IL_{am}^{bar}) as shown in [13]. The opposite occurs for *cr* state: most of the signal power is bar transmitted while a small fraction of the signal power is cross transmitted ($IL_{cr}^{cross} \ll IL_{cr}^{bar}$).

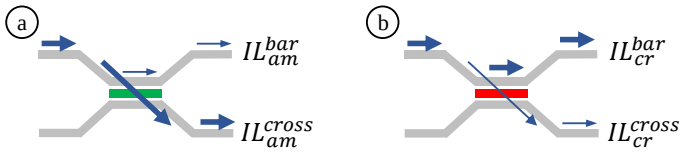

Figure 5: IL for DC according to the state of PCM and output port, a) am: cross transmission of most signal power, b) cr: bar transmission of most signal power

In our model, we do not consider the crosstalk induced by bar and cross transmission through IL_{cr}^{cross} and IL_{am}^{bar} respectively. However, in block/block mode where signal mostly propagates toward the terminator, we consider IL_{cr}^{cross} for the last DC to obtain the ratio of signal propagation to the output. Table 3 summarizes the ring transmission parameters according to the selected tuning resonance wavelength and the modulated data. Tuning ring to λ_s (resp. λ_s-Δ_λ) leads to $IL_{\lambda s}$ (resp. $IL_{\lambda s-\Delta\lambda}+ER_{\lambda s-\Delta\lambda}$) and $IL_{\lambda s}+ER_{\lambda s}$ (resp. $IL_{\lambda s-\Delta\lambda}$) for logic inputs of '1' and '0' respectively. When the ring is tuned to $\lambda_s+\Delta_\lambda$, the loss is independent from the data.

Table 3: Ring loss according to the tuning and modulated data

Tuning	Data	
	0	1
λ_s	$(IL)_{\lambda s}+ER_{\lambda s}$	$IL_{\lambda s}$
λ_s - Δ_λ	$IL_{\lambda s-\Delta\lambda}$	$(IL)_{\lambda s-\Delta\lambda}+(ER)_{\lambda s-\Delta\lambda}$
λ_s +Δ_λ	$IL_{\lambda s+\Delta\lambda}$	

4.2 Ring Power

The total ring power is defined by i) the calibration power of modulating rings (i.e. rings which are not bypassed using the directional couplers) ii) the calibration power of ring filters and iii) the modulation power *P_M*, as defined by:

$$P_{ring} = \sum_{i=1}^{I} P_{\lambda s} + \sum_{j=1}^{J} P_{\lambda s-\Delta\lambda} + \sum_{k=1}^{K} P_{\lambda s+\Delta\lambda} + \sum_{l=1}^{I+J} P_M \quad (6)$$

Where *I*, *J* and *K* represent the number of rings calibrated at λ_s, $\lambda_s-\Delta_\lambda$ and $\lambda_s+\Delta_\lambda$ respectively.

4.3 Reconfiguration Power

The configuration of a given function involves changing the state of PCMs (cr→am or am→cr). While the static power consumption depends only on the losses induced by the directional couplers, the dynamic power, $P_{reconfig}$, depends on the PCM state conversion energy E_{sc} and the function reconfiguration frequency *f*. In our model, we first consider the worst-case scenario since i) we assume that all PCM elements change state when a new function is configured and ii) we use the largest of $E_{(cr\rightarrow am)}$ and $E_{(am\rightarrow cr)}$ for the state conversion, as defined by:

$$E_{sc} = max\,(E_{cr\rightarrow am}, E_{am\rightarrow cr}) \quad (7)$$

$$P_{reconfig} = f \times \sum_{i=0}^{number\ of\ PCMs} E_{sc} \quad (8)$$

We also consider a scenario in which we take into account the actual number of PCMs that change state for each possible reconfiguration.

5 Results

In this section, we evaluate the power consumption of the proposed architectures. We first estimate the laser power overhead needed to compensate for losses induced by PCM elements and coupler. We then estimate the impact of the reconfiguration frequency on the cell power efficiency. Table 4 summarizes the considered parameters for micro ring resonator and DC at 1521.5nm wavelength. We assume 0.9mW modulation power (P_M) [10].

Table 4: Cell parameters

Device	Parameter type	Parameter	
MR	Tuning power (mW)	$P_{\lambda s}$	9.9 [10]
		$P_{\lambda s-\Delta\lambda}$	9.7 [10]
		$P_{\lambda s+\Delta\lambda}$	12.9 [10]
	Loss (dB)	$IL_{\lambda s}$	-1.25 [10]
		$ER_{\lambda s}$	-12.25 [10]
		$IL_{\lambda s-\Delta\lambda}$	-1.25 [10]
		$ER_{\lambda s-\Delta\lambda}$	-8.75 [10]
		$IL_{\lambda s+\Delta\lambda}$	0 [10]
DC	Phase transition energy (nJ)	E_{sc}	2 [13]
	Loss (dB)	IL_{cr}^{bar}	-0.16 [13]
		IL_{cr}^{cross}	-13.7 [13]
		IL_{am}^{bar}	-22.9 [13]
		IL_{am}^{cross}	-0.72 [13]

5.1 Cell Insertion Loss

We evaluate the cell insertion loss for each configuration, as reported in Table 5. Pass/pass leads to the lowest loss since the signal propagating from input to the output cross two DCs in the am states. Assuming IL_{am}^{cross}=0.72dB, this leads to 1.44dB total loss. Block/block leads to the 14.42dB loss, i.e. the highest attenuation, by configuring DC_1 and DC_2 in *am* and *cr* states respectively. Pass/block involves using the modulation path, i.e. DC_1 and DC_2 are in *cr* state and ring is tuned to λ_s. Depending on the modulated data, the ring involves an attenuation of $IL_{\lambda s} = 1.25dB$ (data '1') and $IL_{\lambda s}+ER_{\lambda s}$=13.5dB (data '0'). The only difference for block/pass is the ring detuning, which is set to λ_0-Δ_λ. This leads to 1.57dB and 10.32dB loss for data '0' and '1' respectively, thus resulting in high extinction ratio for both modulation modes. Since comparable insertion losses are obtained for all the modes, data '1' on the cell output will be represented by similar power levels. We thus conclude that a same laser power can be used for all the configurations and that no laser power tuning is needed.

Table 5: Cell insertion loss wrt cell configuration

Mode	Device Configuration			IL (dB)	
	DC_1	MR	DC_2		
pass/pass	*am*	NA	*am*	$2 \times IL_{am}^{cross}$	1.44
block/block	*am*	NA	*cr*	$IL_{am}^{cross} + IL_{cr}^{cross}$	14.4
pass/block	*cr*	λ_s	*cr*	$2 \times IL_{cr}^{bar} + IL_{\lambda s}$	1.57
block/pass	*cr*	λ_s-Δ_λ	*cr*	$2 \times IL_{cr}^{bar} + IL_{\lambda s-\Delta\lambda}$	1.57

5.2 Laser Power

In order to estimate the required laser power, we estimate the worst-case loss at the architecture level for each implementation of the non-volatile RDL architecture. Figure 6 illustrates the loss breakdown for each RDL. The worst-case loss occurs for functions in which signal is propagating through two modulating rings such as AB and XOR, which involves $3IL_{cr}^{bar}$ and $2IL_{\lambda s\,/\,\lambda s-\Delta\lambda}$ and results in 2.98dB. For same functions RDL in [10] leads to 2.5dB loss.

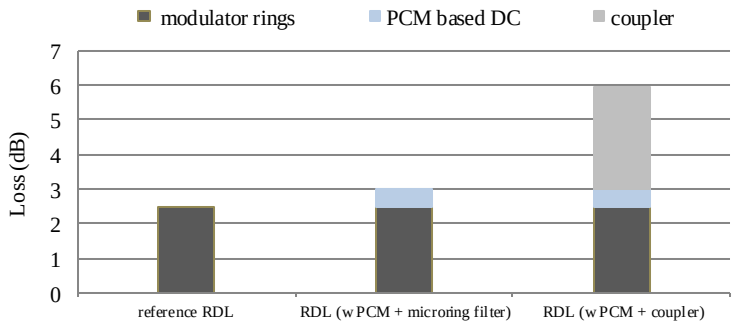

Figure 6: Loss breakdown for RDL architectures

To compensate the 0.48dB and 3.48dB additional loss for RDLs with ring filters and coupler, the injected optical power are set to 2.25mW and 4.5mW respectively. Assuming a 25% lasing efficiency [22], this leads to 1mW and 10mW laser power overhead respectively. In the following, we discuss how energy saving can be achieved for RDL with PCM and ring filters thanks to i) the use of the bypass path, which allows to avoid tuning unused rings. For coupler based RDL extra saving is achieved thanks to the ii) removal of ring filters which reduces MRR calibration power and iii) turning off laser for functions which involves the use of one waveguide such as A and AB.

5.3 Power Saving Analysis

In the following we investigate the power saving of the two implementations of non-volatile architecture wrt RDL in [10] as reported in Figure 7. For functions A and B, three rings out of four are bypassed thanks to the PCM based DC. This results in 35% saving for RDL with ring filters. For coupler based RDL in addition to bypassing rings, turning off the laser on the lower horizontal waveguide and saving the calibration power of ring filters lead to 72% power saving. This is achieved despite of 10mW laser power overhead needed to compensate for the loss induced by DCs and coupler. Functions involving two operands (A+B, AB, AB', A+B') allow bypassing

two rings, thus leading to 22% power saving for RDL with ring filters. For coupler based RDL, functions AB and AB' lead to 61% power saving, while functions A+B and A+B' result in 50% power saving. While in all the above mentioned functions two rings are bypassed and calibration power of ring filters are saved, however turning off laser for functions of AB and AB' leads to extra saving. XOR and XNOR involve the use of all rings. Therefore due to the higher laser power needed to compensate loss induced by PCM, RDL with ring filters leads to slight power increase of (+0.2%). For coupler based RDL calibration power saving of ring filters outperforms the laser power overhead and results in 29% power saving. Therefore while RDL with ring filters leads to 19% average power saving, 53% is obtained for coupler based RDL.
The results demonstrate that using PCM to bypass ring resonators not needed to modulate data lead to significant improvement in the power efficiency. While PCM leads to saving in both implementations of proposed RDLs, keeping laser off for some functions and saving the calibration power of ring filters result in extra saving for coupler based RDL.
While we investigated the use of PCM on the reconfigurable directed logic architecture, we believe that the same approach could be applied to other computing architecture such as OLUT or to reconfigurable nanophotonic interconnects, which we will investigate in our future work.

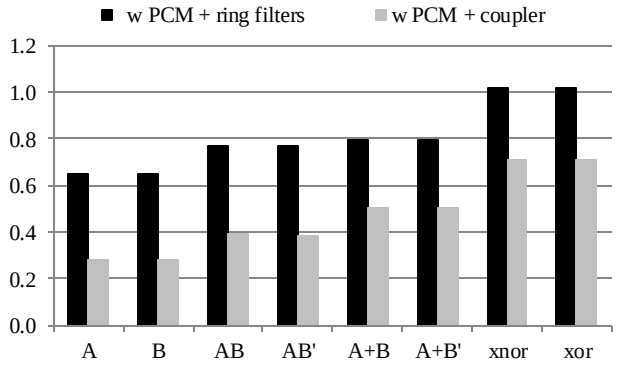

Figure 7: Normalized power of ring filter based and coupler based RDLs wrt RDL in [10]

5.4 Power Saving Analysis Of Coupler Based RDL

In this section we investigate the impact of MRR calibration power and laser efficiency on power saving of coupler based RDL. For this purpose, we consider laser efficiencies of 10% and 25% and we focus the study on functions A+B and XOR, as illustrated in Figure 8 and Figure 9. We assume MRR calibration power ranging from 1mW to 10mW for pass/block mode, which corresponds to the power consumption needed to detune the rings from the signal wavelength. We also consider MRR cali-

bration power for block/pass and pass/pass modes to be respectively 0.2mw below and 3mw above the caliobration power for pass/block mode.

The implementation of A+B with coupler based RDL considering 25% laser efficiency is more power efficient for all considered MRR calibration power, as shown on Figure 8. However, for 10% laser efficiency, the proposed implementation is power efficient from 6mW. Implementation of A+B on coupler based RDL involves saving the calibration power of four filter rings and two modulating rings. However, the PCM also involves laser power overhead. Therefore the architecture is more power efficient when laser efficiency is 25% or MRR calibration power is greater than 6mW.

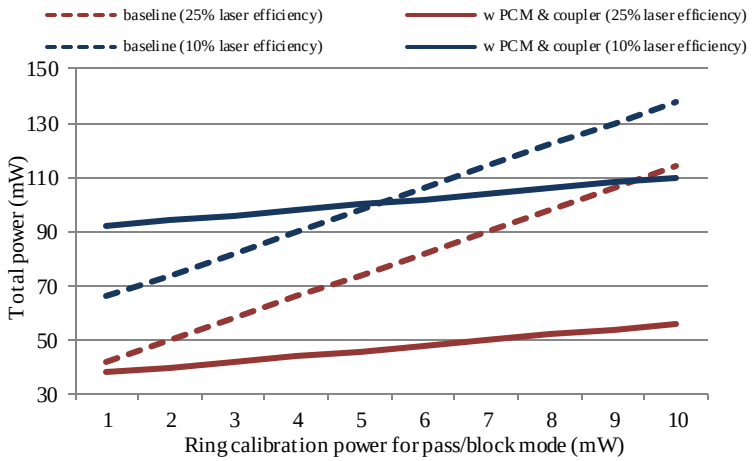

Figure 8: Total power consumption for A+B considering laser efficiencies of 10% and 25%

Figure 9 shows the implementation of XOR on both RDLs. Coupler based RDL is more power efficient from 2mW and 9mW for laser efficiencies of 25% and 10% respectively. Since XOR involves the use of all modulating rings, the coupler based RDL is less efficient for implementation of this function compared with A+B. However considering laser efficiency of 25% makes coupler based RDL a more power efficient candidate for implementation of functions for calibration power ranging from 2mW to 10mW.

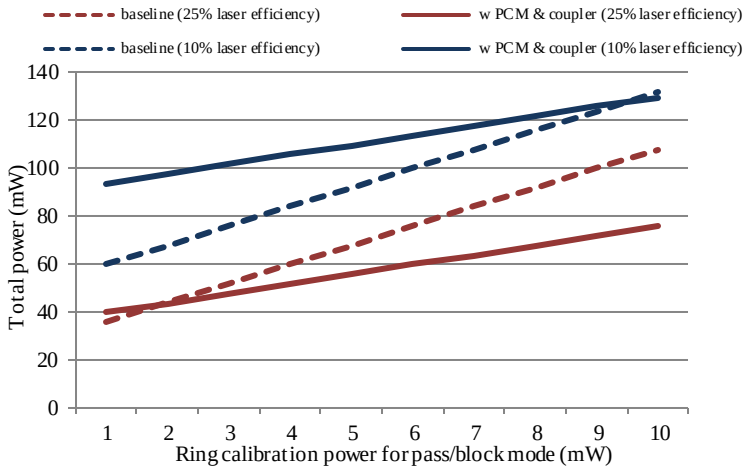

Figure 9: Total power consumption for XOR considering laser efficiencies of 10% and 25%

5.5 Reconfiguration Power

We evaluate the impact of state change of PCM elements according to the architecture reconfiguration frequency. For this purpose, we assume a 2nj [13] energy consumption to change the state of a PCM element. We assume a minimum reconfiguration period of 100ns since, according to [18], the amorphization and crystallization times are in the range of ps to ns. To obtain reconfiguration power two scenarios are considered. First we assume all PCMs are reset between each reconfiguration which leads to the worst case. In second scenario we take into account the actual number of PCMs that change state between each possible reconfiguration. For this purpose we assume that architecture is initially configured for a function then we consider its reconfiguration to all other functions and obtain the number of PCMs that must change state for each reconfiguration as summarized in Table 6.

Table 6: Number of PCMs state changes for each reconfiguration

		Function after reconfiguration							
		A	B	AB	AB'	A+B	A+B'	xnor	xor
Function before reconfiguration	A	-	2	2	2	1	1	3	3
	B	2	-	2	2	3	3	3	3
	AB	2	2	-	0	3	3	1	1
	AB'	2	2	0	-	3	3	1	1
	A+B	1	2	3	3	-	0	4	4
	A+B'	1	2	3	3	0	-	4	4
	xnor	2	2	1	1	4	4	-	0
	xor	2	2	1	1	4	4	0	-

Figure 10 illustrates an example in which the initial function is A+B. Reconfiguring the architecture for A+B' does not require any PCM state change. Only ring tuning on lower waveguide changes from λ to λ-Δ_λ. However implementing XOR requires four of PCMs to be reset and all rings to be tuned. To obtain reconfiguration power we consider the average of all PCM reconfiguration listed in Table 6.

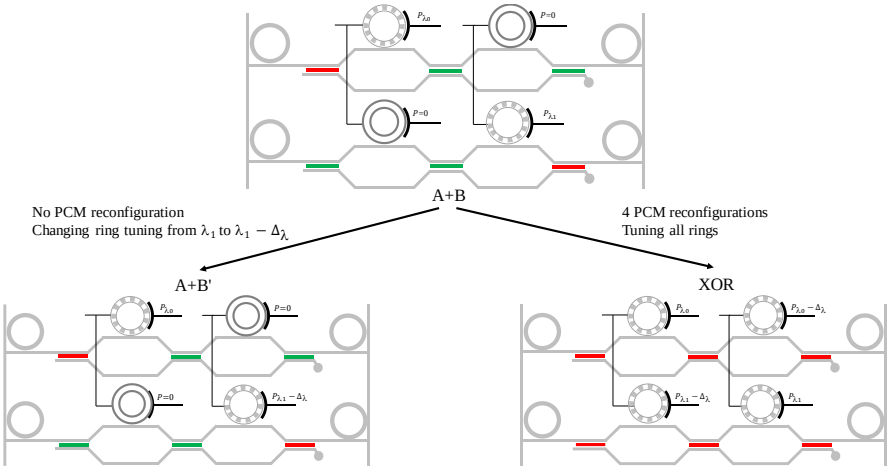

Figure 10: Reconfiguration of architecture to A+B' and XOR considering the initial function of A+B

While average power consumption of all functions for RDL in [10] is 107 mW, the power consumption for PCM based RDL with ring filters and with coupler is 87.3mW and 51mW respectively. Here we investigate the impact of the reconfiguration frequency on total power consumption. Figure 11 illustrates the power consumption for each reconfiguration scenario for two implementation of PCM based RDLs. Both coupler based RDL and ring filter based RDLs are most power efficient when no reconfiguration is required. The higher the reconfiguration frequency the higher the power consumption. Ring filter based RDL is power efficient up to 1.7MHz and 5MHz for worst case and actual scenarios respectively and coupler based RDL is power efficient up to 4.7MHz and 14MHz for corresponding scenarios respectively. This demonstrates that taking into account the current state of PCMs is needed to efficiently reconfigure the architecture. This is especially important when the architecture is extended to process large numbers of inputs, as discussed in the following.

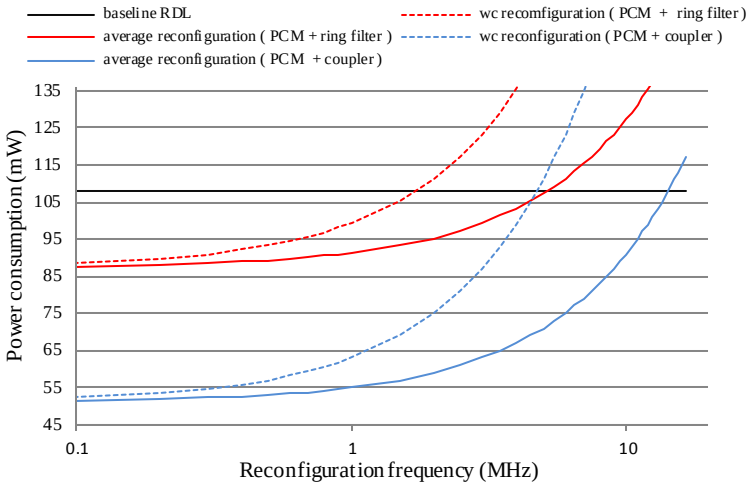

Figure 11: Power consumption according to reconfiguration frequency for PCM based RDLs

5.6 Toward Large Scale Architectures

In this section, we study the usage of the architecture to enable the processing of multi operand functions. From the coupler based architecture, which is the most energy efficient design, we define architecture illustrated in Figure 12. It is essentially composed of two cascaded cores which are interconnected using waveguides linking upper and lower branches of DC_3 and DC_9 to DC_4 and DC_{10}. The other two branches are used to sum the output signals and transmit the results to a photodetector. Therefore, different optical connection between the cores are obtained depending on the PCM configurations. In following we show how sum of products for four operands can be achieved using proposed architecture. We also discuss the limits of the architecture and introduce future works.

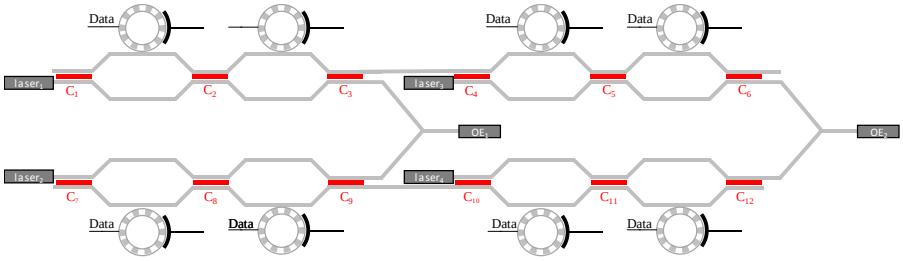

Figure 12: Architecture for processing multi operand functions

Figure 13 illustrates the implementation of ABCD+EFGH. Both ABCD and EFGH are implemented through configuring all cells in pass/block mode. In order to transmit

the signal from first core to the second one, both DC_3 and DC_9 are configured in cr state. This allows to avoid turning on the $laser_3$ and $laser_4$. Signals transmitting from lower and upper waveguides propagate to the OE of second core through configuring DC_6 and DC_{12} in am state. Therefore the sum of products are obtained.

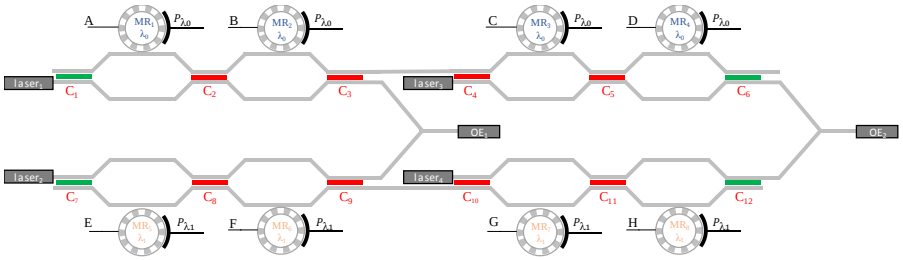

Figure 13: implementation of ABCD+EFGH

Although the cascading of computing cores using PCM based directional couplers appear promising, the architectures suffer from several limitations. For instance, the implementation of multi-input XOR cannot be achieved since it requires crossing of data between the cores. While using electro-optical solutions would solve the issue, the use of electronics would also considerably limit the advantages of the such architectures. Hence, topologies involving heterogeneous and specialized cores [17] [23] are probably needed. Another challenge remains the losses induces by PCM material; while we have shown that crossing relatively small number (<10) of PCM based directional couplers doesn't have a significant impact on the required laser power, the power consumption of large circuits involving hundreds or thousands of PCM may be dominated by static power. This will call for synthesis tools enabling the mapping of functions to minimize the crossing of PCMs [24]. Finally, as already previously discussed, PCM suffers from a limited endurance and high reconfiguration time. This will call for synthesis tools able to map the application while taking into account the current PCM state to minimize changes of states.

6 CONCLUSION

In this chapter, we investigate two implementations of non-volatile PCM based RDL defined as ring filter based RDL and coupler based RDL. Both involve the use of PCM to bypass unused microring resonator. Ring filter based RDL includes MRR to direct WDM signal to horizontal waveguide and to direct the modulated signal to the photodetector where OE conversion occurs. In coupler based RDL lasers are placed on each waveguide allowing to turn it off when signal is not used. The modulated signals of waveguides are merged through coupler. Bypassing MRRs in ring filter based RDL leads to 19% of saving in power consumption compared with baseline. Coupler based RDL results in 53% saving due to the reduced MRR calibration power

of ring filters in addition to bypassing of non-modulating rings. We also investigate the impact of the PCM reconfiguration frequency on total power consumption considering two reconfiguration scenarios. Results show that as the reconfiguration frequency is decreased the architectures are more power efficient. Considering current state of PCM leads to reduced number of required PCM reconfiguration which leads to actual assumption of the reconfiguration power. We also investigated the cascading of the architecture to enable multi operand function. The architecture is extended to involve the AND of multi operands without opto-electronic conversion. The drawback however is its limitation in implementing XOR, which requires the electrical connection between cores which we intend to investigate in more details in future.

7 Acknowledgment

This research was supported by the Fonds de recherche du Québec – Nature et technologies (FRQNT) under grant 2021-NC-286424.

References

1. A.H. Atabaki, S. Moazeni, F. Pavanello, et al. "Integrating photonics with silicon nanoelectronics for the next generation of systems on a chip," Nature 556, 349–354 , 2018.
2. B. Jalali, M. Paniccia and G. Reed, "Silicon photonics," IEEE Microwave Magazine, vol. 7, no. 3, pp. 58-68, June 2006.
3. S. Xu, J. Wang, R. Wang, J. Chen, and W. Zou, "High-accuracy optical convolution unit architecture for convolutional neural networks by cascaded acousto-optical modulator arrays," Opt. Express 27, 19778-19787, 2019.
4. R. A. Minasian, "Photonic signal processing of microwave signals," IEEE Transactions on Microwave Theory and Techniques, vol. 54, no. 2, pp. 832-846, 2006.
5. Z. Zhao, Z. Wang, Z. Ying, S. Dhar, R. T. Chen and D. Z. Pan, "Optical computing on silicon-on-insulator-based photonic integrated circuits," IEEE 12th International Conference on ASIC (ASICON), Guiyang, China, pp. 472-475, 2017.
6. Z. Ying, Z. Wang, Z. Zhao, S. Dhar, D. Pan, R. Soref, and R. Chen, "Silicon microdisk-based full adders for optical computing," Opt. Lett. 43, 983-986 , 2018.
7. Z. Li, S. Le Beux, C. Monat, X. Letartre and I. O'Connor, "Optical Look Up Table," Design, Automation & Test in Europe Conference & Exhibition (DATE), Grenoble, France, pp. 873-876, 2013.
8. Y. Tian et al., "Reconfigurable Electro-optic Logic Circuits Using Microring Resonator-Based Optical Switch Array," IEEE Photonics Journal, vol. 8, no. 2, pp. 1-8, 2016.
9. Q. Xu and R. Soref, "Reconfigurable optical directed-logic circuits using microresonator-based optical switches," Opt. Express 19, 5244-5259, 2011.
10. C. Qiu, W. Gao, R. Soref, J. Robinson, and Q. Xu, "Reconfigurable electro-optical directed-logic circuit using carrier-depletion micro-ring resonators," Opt. Lett. 39, 6767-6770, 2014.
11. I. Chakraborty, G. Saha, A. Sengupta, et al. "Toward Fast Neural Computing using All-Photonic Phase Change Spiking Neurons," Sci Rep 8, 12980 , 2018.

12. S. Abdollahramezani, O. Hemmatyar, H. Taghinejad, A. Krasnok, Y. Kiarashinejad, M. Zandehshahvar, A. Alù, A. Adibi. "Tunable nanophotonics enabled by chalcogenide phase-change material," Nanophotonics, 9(5), 1189-1241. 2020.
13. P. Xu, J. Zheng, J. Doylend, A. Majumdar, "Low-Loss and Broadband Nonvolatile Phase-Change Directional Coupler Switches," ACS Photonics ,6(2), 553 - 557, 2019.
14. T. Ishihara, A. Shinya, K. Inoue, K. Nozaki and M. Notomi, "An integrated optical parallel adder as a first step towards light speed data processing," International SoC Design Conference (ISOCC), Jeju, Korea, pp. 123-124, 2016.
15. J. Shiomi, T. Ishihara, H. Onodera, A. Shinya and M. Notomi, "An Integrated Optical Parallel Multiplier Exploiting Approximate Binary Logarithms Towards Light Speed Data Processing," IEEE International Conference on Rebooting Computing (ICRC), McLean, VA, USA, pp. 1-6, 2018
16. Y. Tian, L. Zhang, and L. Yang, "Electro-optic directed AND/NAND logic circuit based on two parallel microring resonators," Opt. Express 20, 16794-16800 , 2012.
17. L. Zhang, J. Ding, Y. Tian, R. Ji, L. Yang, H. Chen, P. Zhou, Y. Lu, W. Zhu, and R. Min, "Electro-optic directed logic circuit based on microring resonators for XOR/XNOR operations," Opt. Express 20, 11605-11614, 2012.
18. J. Zheng, A. Khanolkar, P. Xu, S. Colburn, S. Deshmukh, J. Myers, J. Frantz, E. Pop, J. Hendrickson, J. Doylend, N. Boechler, and A. Majumdar, "GST-on-silicon hybrid nanophotonic integrated circuits: a non-volatile quasi-continuously reprogrammable platform," Opt. Mater. Express 8, 1551-1561 , 2018.
19. C. Ríos, M. Stegmaier, P. Hosseini, et al. "Integrated all-photonic non-volatile multi-level memory," Nature Photon 9, 725–732, 2015.
20. Y. Ikuma, T. Saiki, H. Tsuda, "Proposal of a small self-holding 2× 2 optical switch using phase-change material," IEICE Electronics Express, 5(12), 442-445, 2008.
21. C. Sun et al., "DSENT - A Tool Connecting Emerging Photonics with Electronics for Opto-Electronic Networks-on-Chip Modeling," IEEE/ACM Sixth International Symposium on Networks-on-Chip, Lyngby, Denmark, pp. 201-210, 2012.
22. P. Zolfaghari and S. L. Beux, "A Reconfigurable Nanophotonic Architecture based on Phase Change Material," 2021 IFIP/IEEE 29th International Conference on Very Large Scale Integration (VLSI-SoC), 1-6, 2021.
23. L. Zhang, R Ji, Y Tian, et al. "Simultaneous implementation of XOR and XNOR operations using a directed logic circuit based on two microring resonators," Opt Express. 6524-40, 2011
24. Z. Zhao, Z. Wang, Z. Ying, et al. "Logic synthesis for energy-efficient photonic integrated circuits," 23rd Asia and South Pacific Design Automation Conference (ASP-DAC), pp. 355-360, 2018